Journal of Power Sources 267 (2014) 235–242

Contents lists available at ScienceDirect

Journal of Power Sources

journal homepage: www.elsevier.com/locate/jpowsour

Hybrid MnO_2/carbon nanotube-VN/carbon nanotube supercapacitors

Y. Su, I. Zhitomirsky*

Department of Materials Science and Engineering, McMaster University, 1280 Main Street West, Hamilton, Ontario L8S 4L7, Canada

HIGHLIGHTS

- VN/multiwalled carbon nanotube (MWCNT) fibrous composites were fabricated.
- VN/MWCNT composites showed good capacitive behavior in Na_2SO_4 electrolyte.
- Good capacitive behavior and cycling stability were achieved at high electrode mass.
- Quartz crystal microbalance data provide an insight into the charging mechanism.
- Aqueous MnO_2/MWCNT-VN/MWCNT supercapacitors were tested in a voltage window of 1.8 V.

GRAPHICAL ABSTRACT

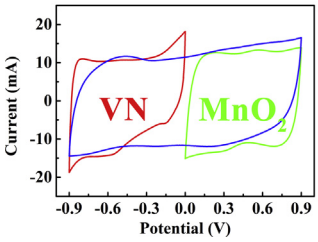

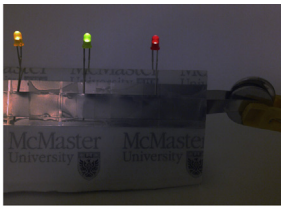

ARTICLE INFO

Article history:
Received 25 January 2014
Received in revised form
14 May 2014
Accepted 17 May 2014
Available online 27 May 2014

Keywords:
Supercapacitor
Hybrid
Carbon nanotube
Vanadium nitride
Manganese dioxide
Composite

ABSTRACT

Composite materials, containing fibrous VN nanoparticles and multiwalled carbon nanotubes (MWCNT) are prepared by a chemical method for application in electrochemical supercapacitors. We demonstrate for the first time that VN-MWCNT electrodes exhibit good capacitive behavior in 0.5 M Na_2SO_4 electrolyte in a negative voltage window of 0.9 V. Quartz crystal microbalance studies provide an insight into the mechanism of charge storage. Composite VN-MWCNT materials show significant improvement in capacitance, compared to individual VN and MWCNT materials. Testing results indicate that VN-MWCNT electrodes exhibit high specific capacitance at high mass loadings in the range of 10–30 mg cm^{-2}, good capacitance retention at scan rates in the range of 2–200 mV s^{-1} and good cycling stability. The highest specific capacitance of 160 F g^{-1} is achieved at a scan rate of 2 mV s^{-1}. The new findings open a new and promising strategy in the fabrication of hybrid devices based on VN. The proof-of-principle is demonstrated by the fabrication of hybrid supercapacitor devices based on VN-MWCNT negative electrodes and MnO_2 –MWCNT positive electrodes with voltage window of 1.8 V in aqueous 0.5 M Na_2SO_4 electrolyte. The hybrid VN-MWCNT/MnO_2-MWCNT supercapacitor cells show promising capacitive and power-energy characteristics.

1. Introduction

Electrochemical supercapacitors based on MnO_2 electrode materials [1–3] are currently attracting significant interest due to the high specific capacitance (SC) in aqueous electrolytes and low cost of MnO_2. The SC of 1380 F g^{-1}, reported for very thin MnO_2 films with mass loading of 5 μg cm^{-2}, was very close to the theoretical

* Corresponding author. Tel.: +1 (905) 525 9140.
E-mail address: zhitom@univmail.cis.mcmaster.ca (I. Zhitomirsky).

http://dx.doi.org/10.1016/j.jpowsour.2014.05.091
0378-7753/

value [4]. However, due to the low electronic and ionic conductivity of MnO_2, the SC decreased significantly with increasing electrode mass [4–7]. Many investigations were focused on the development of nanostructured MnO_2 electrodes and composites with advanced microstructure and enhanced performance [8–10]. Composite MnO_2 – carbon nanotube electrodes [11–15] showed improved SC compared to pure MnO_2. The specific capacitance of 155 F g^{-1} was achieved for active material loading of 40 mg cm^{-2} in a voltage window of 1 V in 0.5 M Na_2SO_4 electrolyte [16].

Hybrid electrochemical cells were developed in order to increase the voltage window of MnO_2 based supercapacitors [17–19]. Good electrochemical performance was achieved using activated carbon as a negative electrode and MnO_2 as a positive electrode in a voltage window of 2.2 V in K_2SO_4 electrolyte [18]. However, testing results indicated that gas evolution can limit the voltage window for practical applications [18]. The authors tested a 1.5 V capacitor for more than 23,000 cycles and demonstrated good electrochemical performance with negligible gas evolution [18]. The hybrid supercapacitors showed enhanced power-energy characteristics [20]. Various hybrid systems were successfully developed and tested using MnO_2 based positive electrodes and activated carbon [18], graphene [21], carbon nanofiber [22], carbon nanotube [23] and Fe_3O_4 [24] as negative electrodes.

Despite the impressive progress achieved in the fabrication of hybrid supercapacitors, there is a need in the development of new materials with high capacitance in the negative potential range to be used together with positive MnO_2 electrodes in Na_2SO_4 electrolyte. Vanadium nitride (VN) is a promising material [25] for negative electrodes of electrochemical supercapacitors [26]. An SC of 1340 F g^{-1} was reported [25] for 0.25 mg cm^{-2} electrodes in 1 M KOH electrolyte at a scan rate of 2 mV s^{-1} in a voltage window of −1.2–0 V versus Hg/HgO. The VN electrodes offer an advantage of good capacitance retention at high scan rate and high electronic conductivity. However, it was found that SC decreased with increasing mass of VN electrode [25]. The SC of 161 F g^{-1} was reported [27] in 1 M KOH electrolyte at a scan rate of 30 mV s^{-1}. The studies of cycling stability [27] showed that the SC was about 70% of its original value after 400 cycles. Many investigations were focused on the development of new methods of VN synthesis [28–30] and optimization of electrolyte composition [31–34]. It was found [29] that nanostructured VN, prepared by reaction of V_2O_5 and melamine in N_2 at 800 °C, showed an SC of 413 F g^{-1} at a current density of 1 A g^{-1}. The capacitive behavior of VN was compared in various electrolytes, such as 1 M KOH, 1 M H_2SO_4, and 3 M NaCl [32] and the highest capacitance of 186 F g^{-1} was reported for 1 M KOH. In another investigation the capacitive behavior of nanocrystalline VN was compared in 0.5 M H_2SO_4, 2 M $NaNO_3$ and 1 M KOH [33] electrolytes for electrode mass of 4 mg cm^{-2}. The highest capacitance of 273 F g^{-1} was achieved using the 1 M KOH electrolyte. The charge–discharge mechanisms were proposed, involving OH^-, SO_4^{2-} and NO_3^- species. The analysis [31] of capacitive behavior of VN in 0.1 M KOH (SC = 234 F g^{-1}) and 0.1 M $[(C_2H_5)_4N]OH$ (SC = 228 F g^{-1}) showed that OH^- was a key species in the charge storage mechanism.

Efforts to improve electrochemical performance of VN have resulted in the development of composites, containing VN nanowires and carbon nanotubes, which were used for the fabrication of flexible electrodes [35] with material loading of 4 mg cm^{-2}. It was found [36] that dispersion of carbon nanotubes in the VN matrix was of critical importance in order to obtain high surface area of VN material, which showed enhanced electrochemical performance. Three dimensional arrays [37], consisting of multiwalled carbon nanotubes (MWCNT) covered by nanocrystalline VN with mass loading of 0.037 mg cm^{-2} showed an SC of 289 F g^{-1}. However, the capacitance decreased with increasing mass loading. Another interesting approach was based on the use of TiN/VN composite fibers with core shell structure [38]. Hybrid VN/NiO [39,40] devices, containing KOH electrolyte, and VN/VO_x [41] devices, based on LiCl/PVA gel electrolyte, showed promising electrochemical performance.

The goal of this investigation was the development of hybrid cells, containing MnO_2-MWCNT positive electrode and VN-MWCNT negative electrode. The proposed method for the fabrication of VN-MWCNT electrodes allowed good electrochemical performance at high mass loadings in the range of 10–30 mg cm^{-2}. The important finding was high SC of negative VN-MWCNT electrodes in 0.5 M Na_2SO_4, which was comparable with SC of the positive MnO_2-MWCNT electrode in the same electrolyte. The high mass loading of individual electrodes was beneficial for the fabrication of hybrid devices, which showed good electrochemical performance in a voltage window of 1.8 V.

2. Experimental procedures

2.1. Materials

Vanadium pentoxide (V_2O_5), melamine ($C_3H_6N_6$), oxalic acid ($H_2C_2O_4$), potassium permanganate ($KMnO_4$), polyvinyl butyral (PVB) (Aldrich) and MWCNT (Arkema) were used as starting materials without further purification. Ni foam (95% porosity, thickness 1.5 mm) current collectors were supplied by Vale company. The method for the fabrication of VN from V_2O_5 and melamine was similar to that described in the literature [29,33]. In a typical procedure 0.5 g of V_2O_5 was dissolved in 80 mL of 0.14 M oxalic acid aqueous solution. After drying, the obtained powder was mixed with 2.5 g of melamine and annealed at 800 °C in N_2 gas atmosphere during 3 h. This procedure was modified for the fabrication of a composite, containing VN (67 mass%) and MWCNT (33 mass%). In the modified procedure, MWCNT were dispersed in the oxalic acid solution, containing dissolved V_2O_5, using ultrasonication. After drying and mixing with melamine the obtained material was annealed at 800 °C in N_2 gas atmosphere during 3 h.

MnO_2 nanoparticles with an average particle size of 30 nm were prepared by the reduction of aqueous $KMnO_4$ solutions using the method described in a previous investigation [42]. MnO_2 was mixed with MWCNT in a mass ratio of 1:1.

2.2. Fabrication of electrodes and cells

The VN/MWCNT(2/1) and MnO_2/MWCNT(1/1) powders were used for the fabrication of slurries in ethanol, containing 5 mass % of PVB binder. The slurries were used for the impregnation of Ni foam current collectors. The impregnated current collectors were dried in air during 12 h and then pressed to 20% of original thickness. The mass of the impregnated material was 10–30 mg cm^{-2}. The testing results presented in the experimental part showed that selected MWCNT content in the electrodes allowed comparable capacitances of the individual electrodes. The composite electrodes, separated by a porous polyethylene membrane (mean pore size 0.4 μm, Vale, Canada) were combined for the fabrication of coin cells (CR2032 type, MTI corporation, USA), which were sealed using a hydraulic crimping machine (MSK-110, MTI Corporation, USA).

2.3. Characterization techniques

Electron microscopy studies were performed using JEOL JSM-7000F scanning electron microscope (SEM). X-ray diffraction (XRD) investigations were carried out using Bruker D8 diffractometer and Co Kα radiation.

Quartz crystal microbalance studies were performed using a microbalance (QCM 922, Princeton Applied Research) controlled by a computer. The mass changes of the quartz resonators were

calculated using Sauerbrey's equation [43,44]. The electrochemical cell contained Au coated 9-MHz quartz resonator with area of 0.2 cm^2 and a Pt counter electrode. The quartz resonators were coated using 1 μL of suspension, containing 5 mg of VN-MWCMT composite and 5% PVB binder, dissolved in 1 mL of ethanol. The suspension was cast on the resonator and dried in oven. The QCM studies were performed in the galvanostatic mode, using positive and negative pulses with constant current of 0.1 mA.

Capacitive behavior and electrochemical impedance of the electrodes were investigated in 0.5 M Na_2SO_4 aqueous solutions. Cyclic voltammetry (CV) studies of individual electrodes and coin cells were performed at scan rates of 2–100 mV s^{-1} using a potentiostat (PARSTAT 2273, Princeton Applied Research). Surface area of the working electrode was 1 cm^2. The three electrode cells contained a platinum gauze counter electrode and a standard calomel reference electrode (SCE). The total capacitance $C = Q/\Delta V$ was calculated using half the integrated area of the CV curve to obtain the charge (Q), and subsequently dividing the charge by the width of the potential window (ΔV). The mass-normalized SC ($C_m = C/m$, m-sample mass) and area-normalized SC ($C_s = C/S$, S-sample area), calculated from the CV data, were investigated. The electrochemical impedance spectroscopy (EIS) studies of complex impedance $Z^* = Z' - iZ''$ were conducted in the frequency range of 10 mHz–100 kHz at the amplitude of the alternating current signal of 5 mV. The complex capacitance $C^* = C' - iC''$ [45] was calculated from the impedance data as $C' = Z''/\omega|Z|^2$ and $C'' = Z'/\omega|Z|^2$, where $\omega = 2\pi f$, f – frequency. A commercial ZSimpWin software (Princeton Applied Research) was used for the simulation of the EIS data using equivalent circuits. Charge–discharge behavior of the coin cells was investigated using a battery analyzer (BST8, MTI corporation, USA).

3. Results and discussion

Fig. 1(A) shows an SEM image of the V_2O_5 powder, used in this investigation. The particle size of V_2O_5 was in the range of 0.2–1.0 μm. The SEM image of the VN powder (Fig. 1(B)) showed that primary particle size is on the nanometric scale. However, some particles formed agglomerates. The size of the agglomerates was comparable with the size of V_2O_5 particles (Fig. 1(A)), used for the synthesis of VN. Such agglomerates were not observed in the SEM images of VN-MWCNT composites. Fig. 1(C) shows a typical SEM image of a VN-MWCMT composite. The microstructure of the composite included fibrous nanoparticles of VN, which had smaller diameter, compared to the diameter of MWCNT. The XRD studies confirmed the formation of a pure VN phase. The XRD pattern of VN corresponds to the JCPDS 35-0768 file (Fig. 1(D)).

The VN electrodes with mass loading of 15 mg cm^{-2} showed a C_m of 38.5 F g^{-1} ($C_s = 0.58$ F cm^{-2}) in 0.5 M Na_2SO_4 electrolyte at a scan rate of 2 mV s^{-1}. The MWCNT electrodes of the same mass showed a C_m of 49.8 F g^{-1} ($C_s = 0.75$ F cm^{-2}). The SC decreased with increasing scan rate due to diffusion limitations of the electrolyte in pores. The VN-MWCNT composite electrode with mass loading of 15 mg cm^{-2} showed C_m of 160.3 F g^{-1} ($C_s = 2.4$ F cm^{-2}) at a scan rate of 2 mV s^{-1}. The SC decreased with increasing scan rate, showing $C_m = 65$ F g^{-1} ($C_s = 0.97$ F cm^{-2}) at a scan rate of 100 mV s^{-1}. The corresponding CVs, used for SC calculations are presented in Fig. 2(B). Nearly box shape CVs indicated good capacitive behavior in the voltage window of −0.9–0 V versus SCE. The increase in current with increasing scan rate indicated good capacitance retention. The higher SC of the composite, compared to VN electrode, can be attributed to lower agglomeration of VN particles and higher conductivity of the VN-MWCNT composite. It is suggested that the MWCNT network provided improved electronic conductivity of the composite material, which was beneficial for the charge–discharge reactions. The EIS data presented in a Nyquist plot of Z″ versus Z′ showed nearly linear dependence. The line slope was less than 90° due to resistance $R = Z'$, which was attributed to electrolyte resistance, electrode material resistance and charge transfer resistance. The Nyquist plot was simulated using an equivalent circuit shown in the inset of Fig. 2(C), which included two R-Q transmission lines, describing the porous electrode [46,47]. In this circuit, R_1, R_2 and R_3 represented the electrolyte resistance, electrode material resistance and charge transfer resistance, respectively. Q_1 and Q_2 elements represent pseudocapacitance and double-layer capacitance [48,49], respectively, with

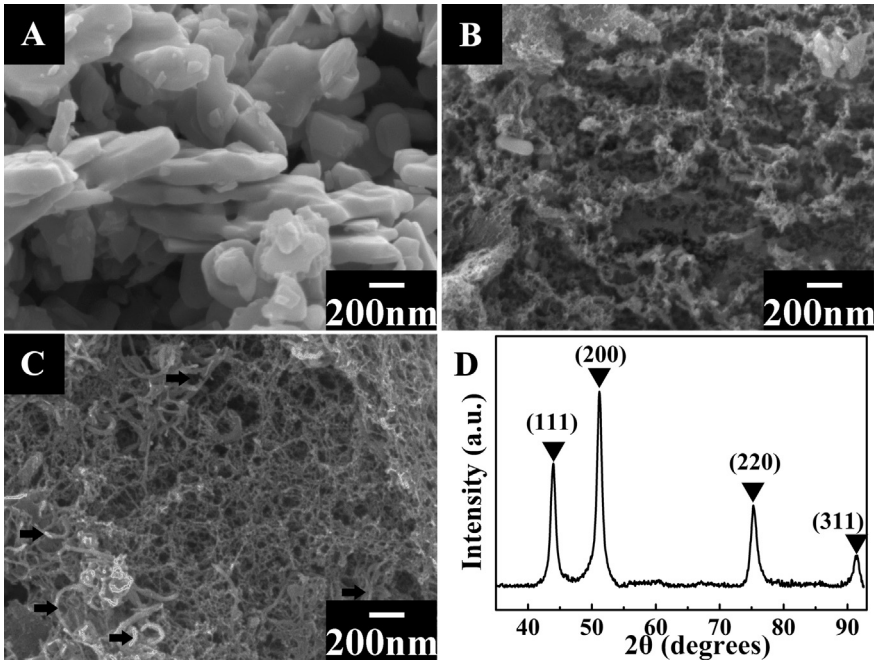

Fig. 1. SEM images of (A) V_2O_5, (B) VN, (C) VN-MWCNT composite, arrows show MWCNT, and (D) XRD spectrum of VN, ▼- peaks corresponding to JCPDS 35-0768 file.

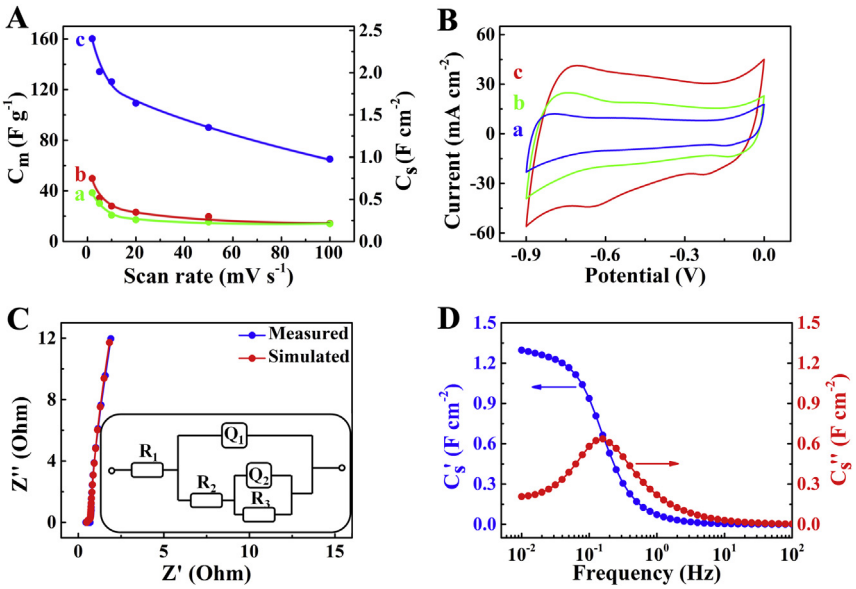

Fig. 2. (A) C_m and C_s versus scan rate for (a) VN, (b) MWCNT, and (c) VN-MWCNT composite electrodes, (B) CVs for VN-MWCNT electrode at scan rates of (a) 5, (b) 10, and (c) 20 mV s^{-1}, (C) Nyquist plot of complex impedance and corresponding simulation data for the VN-MWCNT composite electrode, inset shows the equivalent circuit used for the simulation, (D) real and imaginary components of capacitance for the VN-MWCNT composite electrode, calculated from the impedance data. Mass loading for all electrodes is 15 mg cm^{-2}.

consideration of surface roughness and capacitance dispersion of interfacial origin. Fig. 2(D) shows frequency dependence of components of the AC capacitance, calculated from the EIS data. The electrodes showed a C_s' of 1.3 F cm^{-2} at a frequency of 0.01 Hz, comparable with C_s, calculated from the CV data at a similar charge–discharge period. The spectrum revealed relaxation type of dispersion [50,51] at frequencies above 0.1 Hz, as indicated by the reduction of C_s' with increasing frequency and corresponding maximum in C_s'' at 0.2 Hz.

The investigation of the cycling behavior of the VN-MWCNT electrodes showed that capacitance increased by 15.9% after 1000 cycles (Fig. 3(A)). The inset in Fig. 3(A) shows increased area of the CV after 1000 cycles. Similar capacitance increase was observed for other materials, it was attributed to microstructure changes during cycling [50]. The analysis of the impedance data (Fig. 3(B)) showed small changes in Z′ and Z″ during cycling. The corresponding low frequency C_s' and C_s'' values increased slightly during cycling (Fig. 3(C,D)). The increase in C_s' with increasing cycle number (Fig. 3(C)) was in agreement with C_s increase (Fig. 3(A)). No obvious frequency shift was observed for the peaks of C_s'', indicating that cycling had no influence on the frequency dependence of AC capacitance.

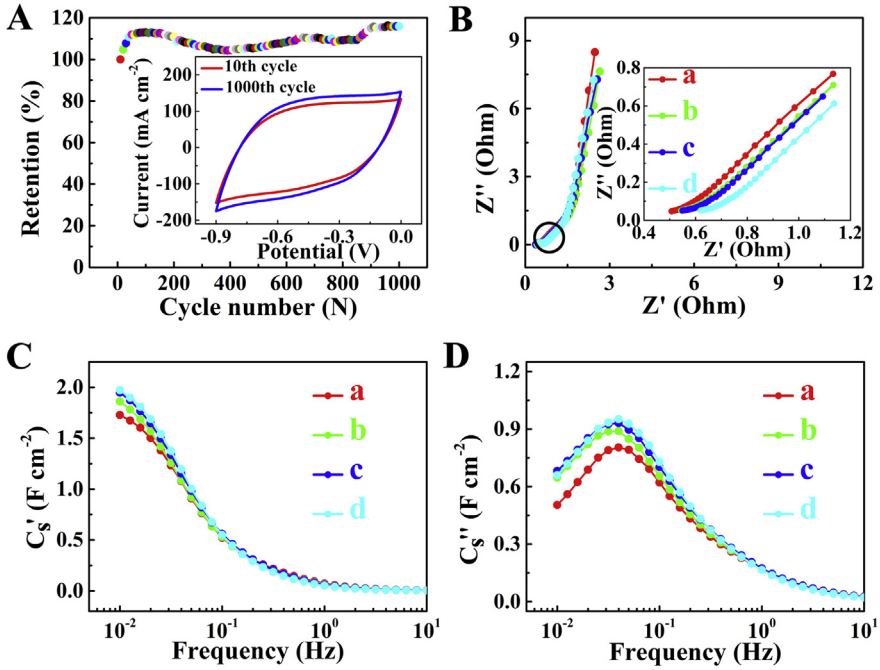

Fig. 3. (A) Capacitance retention for 30 mg cm^{-2} VN-MWCNT composite electrode at a scan rate of 50 mV s^{-1}, inset shows CVs for 10th and 1000th cycles. (B) Nyquist plot of complex impedance, inset shows encircled high frequency range, (C) C_s', and (D) C_s'', calculated from the impedance data after (a) 250th, (b) 500th, (c) 750th, and (d) 1000th cycle.

Previous investigations showed good cycling stability of VN electrodes in KOH electrolyte at low active mass loadings (0.21–0.41 mg cm^{-2}) [25]. The capacitance reduction was less than 10% after 1000 cycles a scan rate of 50 mV s^{-1}. In another investigation [29] the capacitance remained at the level of 60% of initial capacitance after 1000 cycles in KOH electrolyte. The VN functionalized carbon nanotube electrodes with VN loading of 0.135 mg cm^{-2} showed [37] capacitance retention of 64% after 600 cycles in a KOH electrolyte at a scan rate of 50 mV s^{-1}. However, it is important to achieve good electrochemical performance and cycling stability at materials loading of 10–20 mg cm^{-2}, which is desired for many commercial devices [52,53]. The good capacitance retention, achieved at material loading of 30 mg cm^{-2} in Na_2SO_4 electrolyte (Fig. 3), is promising for practical application of VN electrodes in electrochemical supercapacitors.

The charging mechanism of VN in the 0.5 M Na_2SO_4 electrolyte is different from that, described for the 1 M KOH electrolyte [25,33,36,40]. In the concentrated KOH solutions, the anionic OH^- species were involved in charge storage in the VN electrodes at negative electrode potentials. The suggested charge storage mechanisms included the double layer formation and Faradaic reactions [25,33]. Numerous XPS studies revealed the formation of surface oxides on VN nanoparticles [25,33,36,40] in aqueous solutions. It was suggested [25] that in the presence of OH^-ions, the following reactions occur on the oxy-nitride surface:

$$VN_xO_y + OH^- \leftrightarrow VN_xO_y \| OH \quad (1)$$

$$VN_xO_y + OH^- \leftrightarrow VN_xO_y - OH \quad (2)$$

Equations (1) and (2) describe double layer ($VN_xO_y\|OH$) and pseudocapacitance, respectively. The pseudocapacitance mechanism involved the electron transfer across the surface. Such mechanisms cannot explain the charge storage of VN in the Na_2SO_4 solutions due to the low concentration of OH^- ions. Moreover, it is important to note that the electric field moves OH^- ions away from the negative electrodes. The analysis of ion migration in supercapacitor electrode material is important for understanding the charge–discharge mechanisms. The QCM technique is an important tool for the analysis of ionic fluxes into porous electrode materials of electrochemical supercapacitors [54].

In this investigation the ionic fluxes in the VN-MWCNT electrodes were analyzed using QCM at galvanostatic conditions. Fig. 4 compares the QCM data for VN-MWCNT coated and uncoated quartz resonators for applied positive and negative constant current pulses of 0.1 mA. For coated electrodes, the application of negative current pulses resulted in a mass gain, which can be attributed to the insertion of Na^+ ions into the VN-MWCNT material. The application of positive current pulses resulted in the mass loss, attributed to electromigration of Na^+ in opposite direction. Literature data [54] on QCM analysis of porous electrode materials in periodic electric fields revealed periodic mass gains related to insertion of both: cations and anions. However, the QCM studies [55] of CNT electrodes in neutral aqueous solutions showed that mass gain was observed only when the potential was scanned in the negative direction. Such behavior indicated significant contribution of the cationic transport. Investigations [54–57] demonstrated that relative contributions of cationic and anionic transport to the mass changes of QCM resonator depend on the relative size of cations and anions and point of zero charge of the electrode material. It was demonstrated that negatively charged carbon nanotubes in aqueous solutions promoted cationic transport [55]. As a result, QCM studies revealed mass gain only for the negative scans [55]. A similar mechanism can explain the QCM data for VN-MWCNT coated resonators. As pointed out above, numerous XPS studies revealed the formation of surface oxides on VN nanoparticles [25,33,36,40] in aqueous solutions. It is known [58] that vanadium oxides have low points of zero charge. Therefore, in neutral solutions the negatively charged surface oxide layers of VN can promote a cationic transport.

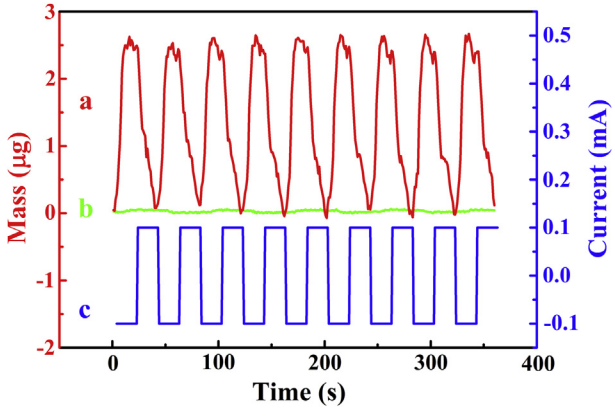

Fig. 4. QCM data for (a) VN-MWCNT coated and (b) uncoated quartz resonators for (c) applied positive and negative constant current pulses of 0.1 mA.

QCM studies of MnO_2 in NaCl and Na_2SO_4 solutions showed mass loss when positive potential was applied to the electrodes [59–61]. However, the results indicated that quantitative analysis of QCM and CV data presents difficulties due to various factors, such as diffusion of cations and anions, influence of scan rate on capacitance and electrolyte electromigration, poor electrolyte access to the bulk of the active material and other factors. The investigations were performed in a wide potential range at different current and voltage conditions. It was suggested that Na cations are involved in the charging of MnO_2 in the positive potential range, according to the following reaction [59,60]:

$$MnO_2Na_\delta \leftrightarrow \delta Na^+ + \delta e^- + MnO_2 \quad (3)$$

The results of QCM studies of the VN electrodes showed that the insertion/deinsertion of Na^+ ions can be involved in the charge–discharge mechanism. The following charging mechanism, involving oxy-nitride surface, can be proposed in the Na_2SO_4 solutions:

$$VN_xO_y + \delta Na^+ + \delta e^- \leftrightarrow VN_xO_yNa_\delta \quad (4)$$

The presented results of the investigation of negative VN-MWVNT electrodes in the Na_2SO_4 electrolyte, coupled with literature data [11–16], demonstrating good electrochemical performance of MnO_2-MWCNT positive electrodes in the same electrolyte, paved the way to the fabrication of hybrid devices with enlarged voltage window.

The VN-MWCNT negative electrodes were combined with MnO_2-MWCNT positive electrodes for the fabrication of supercapacitor cells. Compared with the previous investigations [16,62], the MWCNT content in the MnO_2-MWCNT electrodes was increased to 50% in order to achieve comparable capacitances with VN-MWCNT electrodes at high scan rates. The capacitive behavior of MnO_2-MWCNT electrode is shown in Fig. S1.

The hybrid cells showed box shape CVs at different scan rates, indicating good electrochemical performance in a voltage window of 1.8 V (Fig. 5(A)). The C_s of 1.33 F cm^{-2} was achieved at a scan rate of 2 mV s^{-1} for mass loading of each individual electrode of 10 mg cm^{-2}. The increase in scan rate resulted in decreasing C_s. The hybrid cells showed C_s of 0.48 F cm^{-2} at a scan rate of 100 mV s^{-1} (Fig. 5(B)). The high mass loading allowed significant improvement

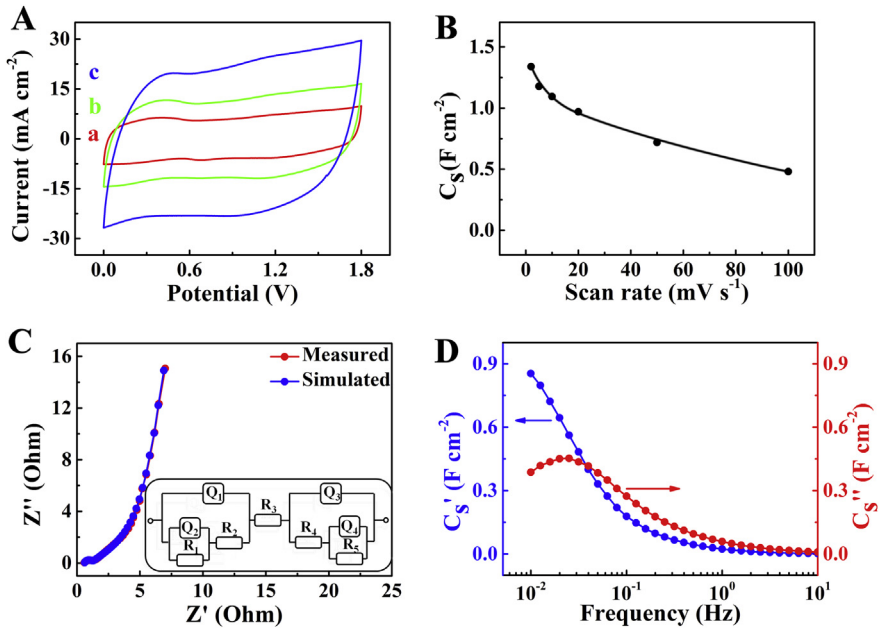

Fig. 5. (A) CVs for two electrode hybrid VN-MWCNT/MnO_2-MWCNT cell at scan rates of (a) 5, (b) 10, and (c) 20 mV s^{-1}, (B) C_s versus scan rate, calculated from the CV data, (C) Nyquist plot of complex impedance for the hybrid cell and corresponding simulation data, the inset shows the equivalent circuit, used for the simulation, (D) C_s', and C_s'', calculated from the impedance data.

in C_s compared to the C_s of 1.85 mF cm^{-2} reported for cell voltage window of 1.3 V [39]. The results of EIS studies of the hybrid cells are presented in the Nyquist plot in Fig. 5(C). The EIS showed relatively low impedance, which is well described by the equivalent circuit, presented in Fig. 5(C) (inset). The equivalent circuit of the device can be considered as a combination of two circuits of individual components, similar to the circuit shown in Fig. 2(C). The circuit includes electrode material resistances (R_2 and R_4) and charge transfer resistances (R_1 and R_5), electrolyte resistance (R_3), pseudocapacitances (Q_1 and Q_3) and double-layer capacitances (Q_2 and Q_4). The capacitance C_s, calculated from the EIS data showed relaxation type frequency dispersion [50,51], as indicated by the rapid decrease in Cs′ in the range of 0.01–0.1 Hz and corresponding maximum in Cs″ at 0.03 Hz (Fig. 5(D)).

Galvanostatic charge–discharge behavior of the hybrid cells was investigated at different current densities in a voltage window of 1.8 V (Fig. 6(A)). As shown in Fig. 6(A), the voltage–time curves were nearly symmetrical at all currents, indicating good Coulombic efficiency related to the reversible redox reactions of both MnO_2 and VN. No significant potential drops at low currents were observed, so the internal resistance was small. The energy density and power density were calculated from the discharges curves and plotted on a Ragone diagram in Fig. 6(B). The maximum energy density was 38.7 Wh kg^{-1} (19.4 mWh cm^{-3}) with a power density of 7.3 W kg^{-1} (3.7 mW cm^{-3}) under discharge current 0.25 mA, which gradually decreased to 13.3 Wh kg^{-1} (6.7 mWh cm^{-3}) with a power density of 316.2 W kg^{-1} (158.1 mW cm^{-3}) under discharge current of 10 mA.

For comparison, the energy and power density, reported [35] for hybrid VN-CNT cells, were of 0.54 mWh cm^{-3} and 0.4 W cm^{-3}, respectively. In another investigation [41], the maximum energy density and power density of 0.61 mWh cm^{-3} and 0.85 W cm^{-3}, respectively, were reported. Therefore, the approach, developed in this investigation allowed significant improvement in power-energy characteristics of the hybrid cells, based on the VN electrode material. The insets in Fig. 6(B) show coin cells, used in this investigation, and LED bulbs powered by the coin cells.

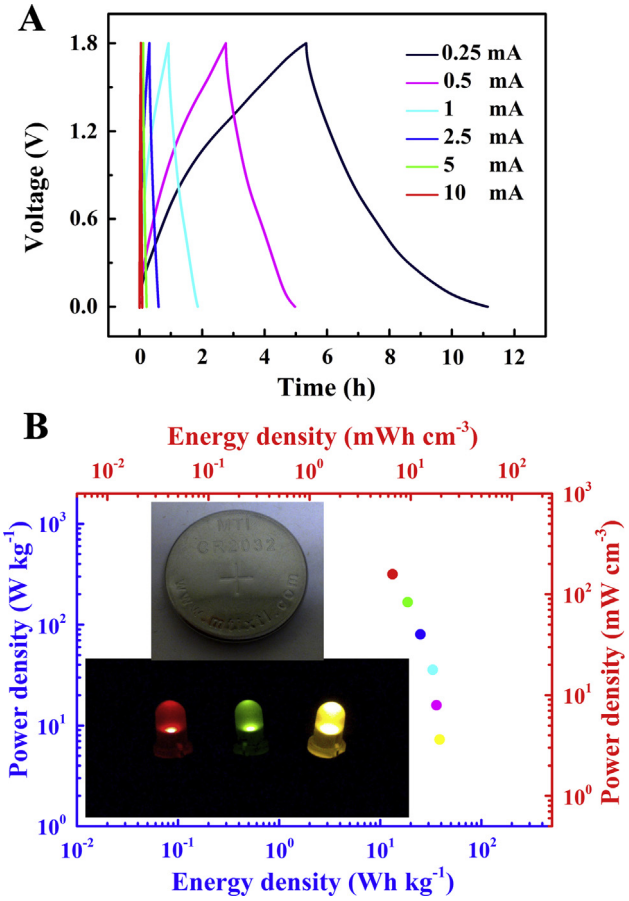

Fig. 6. (A) Galvanostatic charge–discharge for two electrode hybrid VN-MWCNT/MnO_2-MWCNT cell at different currents, (B) Ragone plot for the two electrode cell. The inset shows VN-MWCNT/MnO_2-MWCNT coin cell used for the charge–discharge tests and LED bulbs powered by the coin cells.

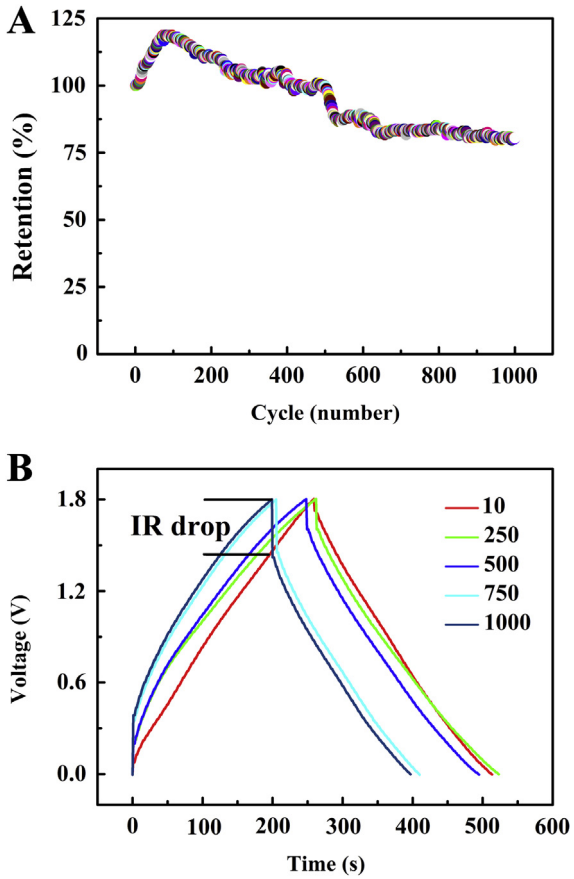

Fig. 7. (A) Capacitance retention for VN-MWCNT/MnO_2-MWCNT cell at constant current of 10 mA, (B) Galvanostatic charge–discharge at a current of 10 mA for different cycles.

The coin cells showed volumetric capacitance of 43 F cm^{-3} (86 F g^{-1}) at a constant current of 0.25 mA cm^{-2}, which is higher than the reported [35] value of 7.9 F cm^{-3} for hybrid VN-CNT cells. The comparison with various commercial supercapacitors [63] indicated that the device developed in this investigation showed higher or comparable power-energy characteristics.

The investigation of cyclic stability of the cells showed capacitance reduction with increasing cycle number. The capacitance retention after 1000 cycles was about 80% (Fig. 7(A)). The capacitance decrease of hybrid cells is not well understood, because individual electrodes showed good capacitance retention in corresponding voltage windows in the same electrolyte. It is suggested that capacitance reduction can be attributed to degradation of electrode materials or separator at operating conditions of 1.8 V. It is known that capacitance reduction during cycling of hybrid capacitors can result from Ref. [64] excessive positive potential on the MnO_2 electrode and electrode matching problems. The analysis of the discharge curves showed that after 200 cycles a voltage drop V = IR appeared at the beginning of discharge (Fig. 7(B)). The voltage drop increased with increasing cycle number and indicated the increasing cell resistance R.

4. Conclusions

Nanostructured VN-MWCNT electrodes for electrochemical supercapacitors, prepared by a chemical method, showed good capacitive behavior in 0.5 M Na_2SO_4 electrolyte. The specific capacitance of VN-MWCNT was significantly higher compared to the capacitance of pure VN and MWCNT materials. QCM studies indicated that charge storage mechanism involves adsorption and desorption of Na^+ ions. The VN-MWCNT electrodes with high mass loading in the range of 10–30 mg cm^{-2} showed high specific capacitance, good capacitance retention in the range of 2–200 mV s^{-1} and good cycling stability. The highest capacitance of 160 F g^{-1} was achieved at a scan rate of 2 mV s^{-1}. Good electrochemical performance of the VN-MWCNT electrodes in the negative potential range in the 0.5 M Na_2SO_4 electrolyte allowed the fabrication of new type of hybrid cells, containing VN-MWCNT negative and MnO_2-MWCNT positive electrodes. The hybrid cells showed promising electrochemical performance in a voltage window of 1.8 V in aqueous 0.5 M Na_2SO_4 electrolyte with energy density of 38.7 Wh kg^{-1} (19.4 mWh cm^{-3} and a power density of 7.3 W kg^{-1} (3.7 mW cm^{-3}).

Acknowledgment

The authors gratefully acknowledge the financial support of the Natural Sciences and Engineering Research Council of Canada and Vale Canada for the donation of Ni foam.

Appendix A. Supplementary data

Supplementary data related to this article can be found at http://dx.doi.org/10.1016/j.jpowsour.2014.05.091.

References

[1] C. Wei, C. Xu, B. Li, H. Du, D. Nan, F. Kang, J. Power Sources 234 (2013) 1–7.
[2] J. Shao, X. Li, Q. Qu, Y. Wu, J. Power Sources 223 (2013) 56–61.
[3] Z. Sun, D. Shu, H. Chen, C. He, S. Tang, J. Zhang, J. Power Sources 216 (2012) 425–433.
[4] M. Toupin, T. Brousse, D. Belanger, Chem. Mater. 16 (2004) 3184–3190.
[5] T. Brousse, M. Toupin, R. Dugas, L. Athouel, O. Crosnier, D. Belanger, J. Electrochem. Soc. 153 (2006) A2171–A2180.
[6] J. Broughton, M. Brett, Electrochim. Acta 49 (2004) 4439–4446.
[7] K.-W. Nam, K.-B. Kim, J. Electrochem. Soc. 153 (2006) A81–A88.
[8] Y. Zhao, P. Jiang, S.-S. Xie, J. Power Sources 239 (2013) 393–398.
[9] Y. Liu, D. Yan, R. Zhuo, S. Li, Z. Wu, J. Wang, P. Ren, P. Yan, Z. Geng, J. Power Sources 242 (2013) 78–85.
[10] M. Yu, T. Zhai, X. Lu, X. Chen, S. Xie, W. Li, C. Liang, W. Zhao, L. Zhang, Y. Tong, J. Power Sources 239 (2013) 64–71.
[11] R. Jiang, T. Huang, Y. Tang, J. Liu, L. Xue, J. Zhuang, A. Yu, Electrochim. Acta 54 (2009) 7173–7179.
[12] H. Xia, C. Huo, Int. J. Smart Nano Mater. 2 (2011) 283–291.
[13] J. Li, I. Zhitomirsky, J. Mater. Process. Technol. 209 (2009) 3452–3459.
[14] H. Fang, S. Zhang, X. Wu, W. Liu, B. Wen, Z. Du, T. Jiang, J. Power Sources 235 (2013) 95–104.
[15] H. Zheng, J. Wang, Y. Jia, C.a. Ma, J. Power Sources 216 (2012) 508–514.
[16] J. Li, Q.M. Yang, I. Zhitomirsky, J. Power Sources 185 (2008) 1569–1574.
[17] T. Brousse, P.-L. Taberna, O. Crosnier, R. Dugas, P. Guillemet, Y. Scudeller, Y. Zhou, F.d.r. Favier, D. Belanger, P. Simon, J. Power Sources 173 (2007) 633–641.
[18] T. Brousse, M. Toupin, D. Belanger, J. Electrochem. Soc. 151 (2004) A614–A622.
[19] C. Shen, X. Wang, S. Li, J.g. Wang, W. Zhang, F. Kang, J. Power Sources 234 (2013) 302–309.
[20] C.-H. Wang, H.-C. Hsu, J.-H. Hu, J. Power Sources 249 (2014) 1–8.
[21] M. Huang, Y. Zhang, F. Li, L. Zhang, Z. Wen, Q. Liu, J. Power Sources 252 (2014) 98–106.
[22] L.-F. Chen, Z.-H. Huang, H.-W. Liang, Q.-F. Guan, S.-H. Yu, Adv. Mater. 25 (2013) 4746–4752.
[23] P.-C. Chen, G. Shen, Y. Shi, H. Chen, C. Zhou, ACS Nano 4 (2010) 4403–4411.
[24] T. Cottineau, M. Toupin, T. Delahaye, T. Brousse, D. Belanger, Appl. Phys. A Mater. Sci. Process. 82 (2006) 599–606.
[25] D. Choi, G.E. Blomgren, P.N. Kumta, Adv. Mater. 18 (2006) 1178–1182.
[26] S. Dong, X. Chen, X. Zhang, G. Cui, Coord. Chem. Rev. 257 (2012) 1946–1956.
[27] X. Zhou, H. Chen, D. Shu, C. He, J. Nan, J. Phys. Chem. Solids 70 (2009) 495–500.
[28] J. Buha, I. Djerdj, M. Antonietti, M. Niederberger, Chem. Mater. 19 (2007) 3499–3505.
[29] D. Shu, C. Lv, F. Cheng, C. He, K. Yang, J. Nan, L. Long, Int. J. Electrochem. Sci. 8 (2013) 1209–1225.
[30] N. Fechler, T.-P. Fellinger, M. Antonietti, Chem. Mater. 24 (2012) 713–719.

[31] P. Pande, P.G. Rasmussen, L.T. Thompson, J. Power Sources 207 (2012) 212–215.
[32] A.M. Glushenkov, D. Hulicova-Jurcakova, D. Llewellyn, G.Q. Lu, Y. Chen, Chem. Mater. 22 (2009) 914–921.
[33] F. Cheng, C. He, D. Shu, H. Chen, J. Zhang, S. Tang, D.E. Finlow, Mater. Chem. Phys. 131 (2011) 268–273.
[34] R.L. Porto, R. Frappier, J. Ducros, C. Aucher, H. Mosqueda, S. Chenu, B. Chavillon, F. Tessier, F. Chevire, T. Brousse, Electrochim. Acta 82 (2012) 257–262.
[35] X. Xiao, X. Peng, H. Jin, T. Li, C. Zhang, B. Gao, B. Hu, K. Huo, J. Zhou, Adv. Mater. 25 (2013) 5091–5097.
[36] C.M. Ghimbeu, E. Raymundo-Pinero, P. Fioux, F. Beguin, C. Vix-Guterl, J. Mater. Chem. 21 (2011) 13268–13275.
[37] L. Zhang, C.M. Holt, E.J. Luber, B.C. Olsen, H. Wang, M. Danaie, X. Cui, X. Tan, V.W. Lui, W.P. Kalisvaart, D. Mitlin, J. Phys. Chem. C 115 (2011) 24381–24393.
[38] X. Zhou, C. Shang, L. Gu, S. Dong, X. Chen, P. Han, L. Li, J. Yao, Z. Liu, H. Xu, Y. Zhu, G. Cui, ACS Appl. Mater. Interfaces 3 (2011) 3058–3063.
[39] E. Eustache, R. Frappier, R.L. Porto, S.d. Bouhtiyya, J.-F. Pierson, T. Brousse, Electrochem. Commun. 28 (2013) 104–106.
[40] Z.-H. Gao, H. Zhang, G.-P. Cao, M.-F. Han, Y.-S. Yang, Electrochim. Acta 87 (2013) 375–380.
[41] X. Lu, M. Yu, T. Zhai, G. Wang, S. Xie, T. Liu, C. Liang, Y. Tong, Y. Li, Nano Lett. 13 (2013) 2628–2633.
[42] M. Cheong, I. Zhitomirsky, Surf. Eng. 25 (2009) 346–352.
[43] M.R. Deakin, D.A. Buttry, Anal. Chem. 61 (1989) 1147A–1154A.
[44] G. Sauerbrey, Zeitschrift für Physik A Hadrons Nucl. 155 (1959) 206–222.
[45] P. Taberna, P. Simon, J.F. Fauvarque, J. Electrochem. Soc. 150 (2003) A292–A300.
[46] B.E. Conway, W.G. Pell, J. Power Sources 105 (2002) 169–181.
[47] Y. Huai, X. Hu, Z. Lin, Z. Deng, J. Suo, Mater. Chem. Phys. 113 (2009) 962–966.
[48] Y. Su, I. Zhitomirsky, J. Colloid Interface Sci. 392 (2013) 247–255.
[49] Y. Su, I. Zhitomirsky, Colloids Surf. A Physicochem. Eng. Aspects 436 (2013) 97–103.
[50] K. Shi, I. Zhitomirsky, J. Power Sources 240 (2013) 42–49.
[51] K. Shi, I. Zhitomirsky, J. Mater. Chem. A 1 (2013) 11614–11622.
[52] L. Wei, G. Yushin, Nano Energy 1 (2012) 552–565.
[53] Y. Gogotsi, P. Simon, Science 334 (2011) 917–918.
[54] M.D. Levi, G. Salitra, N. Levy, D. Aurbach, J. Maier, Nat. Mater. 8 (2009) 872–875.
[55] J.N. Barisci, G.G. Wallace, R.H. Baughman, Electrochim. Acta 46 (2000) 509–517.
[56] S. Sigalov, M.D. Levi, G. Salitra, D. Aurbach, J. Maier, Electrochem. Commun. 12 (2010) 1718–1721.
[57] N. Levy, M.D. Levi, D. Aurbach, R. Demadrille, A. Pron, J. Phys. Chem. C 114 (2010) 16823–16831.
[58] J. Livage, Materials 3 (2010) 4175–4195.
[59] S.-L. Kuo, N.-L. Wu, J. Electrochem. Soc. 153 (2006) A1317–A1324.
[60] S. Devaraj, N. Munichandraiah, Electrochem. Solid State Lett. 12 (2009) F21–F25.
[61] S. Sopcic, R. Peter, M. Petravic, Z. Mandic, J. Power Sources 240 (2013) 252–257.
[62] Y. Wang, Y. Liu, I. Zhitomirsky, J. Mater. Chem. A 1 (2013) 12519–12526.
[63] V.V. Obreja, Phys. E 40 (2008) 2596–2605.
[64] Z.-S. Wu, W. Ren, D.-W. Wang, F. Li, B. Liu, H.-M. Cheng, ACS Nano 4 (2010) 5835–5842.